RSC Advances

PAPER

View Article Online
View Journal | View Issue

CrossMark click for updates

Cite this: *RSC Adv.*, 2016, **6**, 34737

Micro- and mesoscopic structural features of a bio-based choline-amino acid ionic liquid†

Olga Russina,* Serena De Santis and Lorenzo Gontrani

Received 24th January 2016
Accepted 29th March 2016

DOI: 10.1039/c6ra02142e

www.rsc.org/advances

High energy X-ray diffraction data from a bio-based ionic liquid constituted by choline ([cho]) and an amino acid (AA), namely n-leucine ([nle]), are presented and described by means of an atomistic molecular dynamics simulation aiming at extracting detailed structural information at both microscopic and mesoscopic spatial scales. We find that similar to other previously studied analogous systems, a strong, hydrogen bonding driven, cation–anion correlation determines the microscopic structure. While other peculiar correlations exist in this [cho][nle] IL, the medium length alkyl tail of the AA leads to the development of a characteristic polar *vs.* apolar alternation, as a consequence of the alkyl tails segregation into domains, thus delivering the formation of an enhanced level of mesoscopic organization in this IL.

Introduction

Ionic liquids (ILs) represent a class of materials which are attracting a lot of attention in the last couple of decades. ILs are typically composed of an organic cation combined with an organic/inorganic anion; by convention, they are liquid below 100 °C. They are characterized by high thermal and chemical stability, low flammability, and enhanced capability of dissolving different compounds. Their physicochemical properties can be easily modulated for a specific task by making the right choice of chemical composition for the ions, the length of the side alkyl tail, the distribution of polarity or introduction of fluorinated and/or further functionalized moieties.[1,2]

The main interest for ILs is currently represented by their green, environmental friendly nature mostly due to their low vapor pressure. Today ILs are considered as a green replacement for several toxic conventional solvents and find application in green chemistry and sustainable technology, electrochemistry, catalysis, extraction and separation *etc.*[3–6]

However IL's environmental impact, specially toxicity depends strongly on the nature of the constituent cations (mostly) and anions.[7–10] It has been demonstrated that aromatic cations that are frequently used in conventional ILs such as imidazolium and pyridinium are rather toxic towards enzymes, microorganisms, cells and poorly biodegradable. It is then not surprising if in the last few years we witnessed a strong quest towards ILs whose constituents are bio-compatible or, even better, biological compounds. For this reason new subgroups of ILs, composed of biomaterials have been introduced.[11–18] Choline amino acid ionic liquids ([cho][AA]ILs)[17–21] being wholly composed of renewable biomaterials, are attracting a great attention due to their inherent bio-compatibility. They are characterised by excellent physicochemical properties, similarly to the traditional ILs, but combined with low toxicity and very good biodegradability.[16,17,20,21] It has been demonstrated that they are thermally stable (at least up to 90 °C) and perform excellently in the fields of organic synthesis and biomass pretreatment.[19] These properties of [cho][AA] ILs, combined with the their low industrial production cost make them promising candidates for use as environmentally friendly solvents in large-scale applications.

In a recent study, our group has reported an improved synthesis protocol for the production of [cho]-AA ionic liquids, which has several advantages compared to previous methods, including a much shorter preparation time, stoichiometry within 1%, very high yields, high reproducibility and involves no organic solvent, thus being more environment friendly.[18] Several physicochemical properties of the newly synthesized material such as density, viscosity, conductivity have been presented and discussed as a function of the nature of anion and its chemical structure. Recently some reports appeared on the structural properties of AA-ILs, including studies on [cho][ala][22] (where [ala] stands for alanine), [cho][pro][23] (where [pro] stands for proline), and [c2mim][gly], [c2mim][ala] and [c2mim][ser][24] (where [c2mim][gly], [c2mim][ala] and [c2mim][ser] stand for 1-ethyl-3-methylimidazolium, glycine, alanine and serine, respectively). The role of the cation in the structural interactions (choline, 1-ethyl-3methylimidazolum and *N*-methylpiperazinium) in amino acid based ILs has been studied by Herrera *et al.*[25] It has been demonstrated that the ILs with choline cation are characterized by much more extended hydrogen bonding network, even if with similar HB strength.

Department of Chemistry, University of Rome "La Sapienza", P.le A.Moro 5, Rome, Italy. E-mail: olga.russina@uniroma1.it

† Electronic supplementary information (ESI) available: Additional experimental information and partial charges used in the definition of the potential. See DOI: 10.1039/c6ra02142e

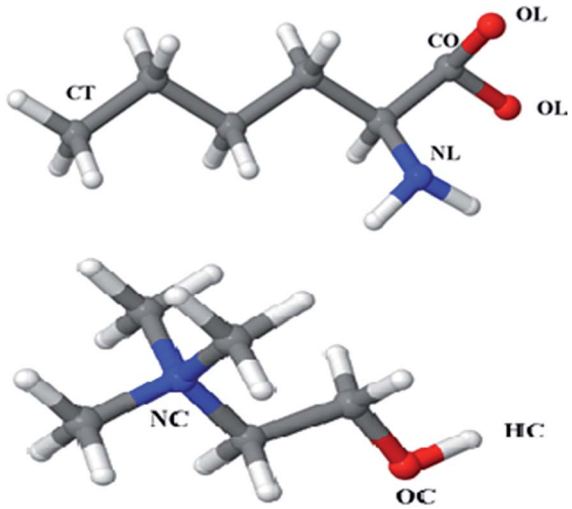

Fig. 1 Chemical structure of choline cation [cho] and norleucine anion [nle].

Here we present the first structural study of the [cho][nle] IL, where norleucine (hereinafter indicated as [nle]), bears a long enough side chain to give rise to the characteristic polar-apolar alternation that characterises the large majority of traditional ILs[26–39] (see Fig. 1). The development of nm-scale domains built up by segregated alkyl tails delivers nano-environments where selectively either polar or apolar compounds can be dissolved simultaneously in the same IL. However the solvation mechanism is more complicate and often non trivial.[40–43] This structural scenario has a major influence on the physicochemical properties such as viscosity, conductivity, density and creates conditions for a range of catalytic, separation, extraction, reaction processes in conventional ILs.[27]

The present study aims at extending the understanding of structural properties in the increasingly relevant class of bio-derived [cho][AA] ILs. We envisage that the occurrence of the same nano-segregated morphology in the present choice of bio-based ILs might further enlarge the range of applications for ionic liquid media.

Experimental session

Synthesis

The synthesis of [cho][nle] was done following the protocol developed by De Santis *et al.*[18] L-norleucine was a Fluka product (purity > 99%), while choline hydroxide (aqueous solution 46 wt%, Sigma) was purchased from Sigma Aldrich. Methanol and acetonitrile were of analytical grade and used without any further purification. Doubly distilled water was used in all experiments. The synthesis is based on a potentiometric method and for further details the reader is addressed to the original publication. The freshly prepared [cho][nle] is characterized by the following parameters: density: 1.05125 g cm^{-3}; viscosity: 6.43 Pa s; conductivity: 20.44 μS cm^{-1}; refractive index: 1.4865. After the synthesis, before the measurements the sample was kept under protective atmosphere, avoiding contact with moisture.

X-ray diffraction data

Wide angle X-ray scattering (WAXS) measurements were collected at room temperature using the non-commercial energy-dispersive X-ray diffractometer (EDXD) built at the Department of Chemistry at the University of Rome Sapienza (Italian Patent no. 01126484-23 June, 1993). A detailed description of instrument, technique, and the experimental protocol of the data acquisition phase, can be found in ref. 44–46. The sample was inserted into a 2 mm quartz cylindrical capillary, after a 72 h drying in high vacuum pump. The diffraction patterns acquired at the different angles were then merged to obtain a continuous spectrum in Q, accessing the range between 0.1 and 19.56 $Å^{-1}$, where Q is the magnitude of the transferred momentum that depends on the scattering angle (2θ), according to the relation $Q = 4\pi/\lambda \sin\theta$.

The total intensity of the radiation scattered by the sample, after corrections for systematic effects (polarization, absorption and incoherent scattering) and rescaling to absolute units (electron units per stoichiometric unit), can be expressed as the sum of the independent atomic scattering from the atoms of the stoichiometric unit, and by $I(Q)$, the static structure factor, that delivers the structural information associated to correlations between atomic species in the sample. $I(Q)$ is given as:

$$I(Q) = \sum_{i=1}^{N}\sum_{j=1}^{N} x_i x_j f_i f_j \rho_0 \int_0^\infty 4\pi r^2 \left(g_{ij}(r) - 1\right) \frac{\sin(Qr)}{Qr}\,\mathrm{d}r \quad (1)$$

where x_i and f_i are the numerical concentrations of the species and their Q-dependent X-ray scattering factors; ρ_0 is the bulk number density of the system. In this study we have used $QI(Q)M(Q)$ form of the structure function, where M is a sharpening factor applied to increase the amplitude of the high Q-portion oscillations.[22,45,46]

$$M(Q) = \frac{f_N^{\,2}(0)}{f_N^{\,2}(Q)} \exp\left(-0.01Q^2\right) \quad (2)$$

The Fourier-transformation of $QI(Q)M(Q)$ delivers the differential distribution function Diff(r)

$$\mathrm{Diff}(r) = \frac{2r}{\pi}\int_0^\infty QI(Q)M(Q)\sin(Qr)\mathrm{d}Q \quad (3)$$

While the experimental functions have been extracted from the diffraction data, the theoretical functions were calculated from the MD trajectories using either in-house purposely written codes or the TRAVIS program.[47–49]

Computational methods

Classical molecular dynamics calculations were executed using the AMBER11 software[50] and a generalized AMBER force field (GAFF),[22,51,52] to generate a suitable model of the systems. The GAFF uses partial atomic charges fitted with the HF/6-31G(d) RESP approach (see ESI†); in this work, similarly to a previous one,[22] we chose to fit the charges using the B3LYP/6-31G(d) electron density and scaling the obtained values by 0.8 to

roughly account for polarization effects. This procedure has been shown to be appropriate for highly charged systems like ionic liquids.[53] The system were simulated in a cubic box (periodic boundary conditions were applied) with box edge = 51.00 Å, leading to a density of 1.02260 g cm^{-3}, as obtained from the preliminary NPT equilibration for the box containing 350 ion pairs. The initial random geometry was generated with PACKMOL.[54] After geometry minimization, a low temperature (50 K) NVT equilibration for 40 ps was applied. The system was then heated at 300 K and a NPT calculation for 5 ns was applied. Before the productive phase, further 2 ns at NVT conditions were executed. A NVT productive phase of 10 ns was then applied with a time step of 2 fs.

The trajectories generated with this protocol were analysed with the TRAVIS software from the Kirchner group.[47–49] Standard analysis approaches involved the calculation of partial radial distribution functions (rdf), angular distribution functions (adf), their combination into combined distribution functions (cdf) and spatial distribution function (sdf). The reader is referred to the Kirchner's literature for further details on these tools.[55]

Results and discussion

Liquid structure

The experimental diffraction data obtained at ambient temperature for the [cho][nle] AA-IL are plotted in Fig. 2, in the form of $QI(Q)M(Q)$, together with the curve obtained from the simulation. The inset shows the theoretical and experimental Diff(r). The agreement is good and comparable to the one observed in previous work on [cho] [ala]-IL.[22] All the relevant experimental diffraction features are accounted for by the model and accordingly we consider the simulated system as representative of the bulk IL structure. We mention that recently a neutron diffraction study on selectively deuterated AA-ILs appeared;[24] the data were modelled using the EPSR approach leading to comparable fitting quality to the present set.

We notice that similarly to the case of the [cho][ala] and other AA-IL, a major diffraction feature is observed at *ca.* 1.3 $Å^{-1}$, that fingerprints correlations associated to intermolecular,[22,24] short close contact distances between ions. Other, higher Q values, peaks in the experimental diffraction pattern essentially correspond to the ones found for other AA-ILs and reflects mostly intramolecular correlations. Noteworthy, while the so far explored AA-ILs did not show diffraction features at Q values shorter than *ca.* 1 $Å^{-1}$, here [cho][nle], whose anion bears a medium length chain, shows a characteristic low Q diffraction feature at *ca.* 0.35 $Å^{-1}$. More evidently this peak is seen in the SAXS data (see Fig. 1 in ESI†).

This feature is ubiquitously found in ILs bearing a long enough apolar chain. In particular this is the second case of long alkyl chain linked to the anion, after the case of alkyl sulfates,[56,57] for which similar low Q features were observed. A more careful discussion of this feature in AA-ILs will be presented later on in this paper: here we just stress that the GAFF potential efficiently describes this scattering feature. Accordingly the simulated system nicely accounts for the mesoscopic order occurring in the present choice of AA-ILs. We stress that this is the first study on the structure of AA-ILs that are characterised by this feature. Recently, an X-ray diffraction study focused on a AA-IL where the AA is proline, an AA bearing a cyclic moiety rather than a linear chain. In that case hints for the existence of polar–apolar alternations, as witnessed by the occurrence of a low Q peak were also observed.[23]

In Fig. 3, we show the Center of Mass (CoM) $g(r)$'s, namely the cation–anion, cation–cation and anion–anion pair correlation functions. These are determined as the $g(r)$'s between those sites that represent cation and anion (C and A, respectively) centres of mass. One can appreciate that together with a strong cation–anion correlation that extends itself up to the second coordination shell, also cation–cation correlations are quite strong; by integration up to the first minimum one can estimate the average number of first neighbours (FN) for each pair. In particular we obtain: FN(C–A) ≈ 6.2, FN(C–C) ≈ 6.0 and FN(A–

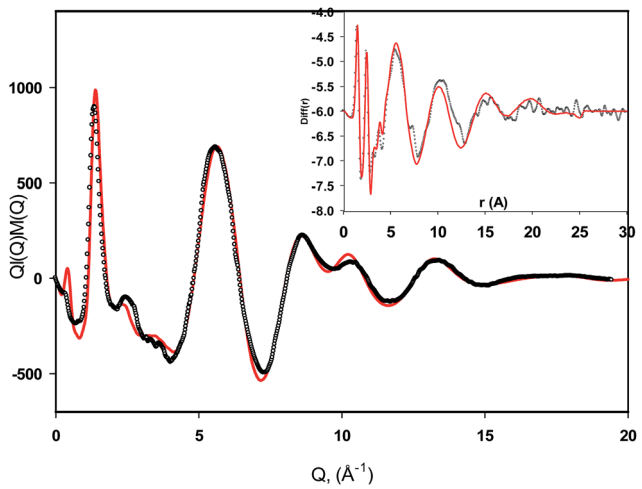

Fig. 2 Experimental and calculated static structure factors in form of $QI(Q)M(Q)$ and Diff(r) (inset) of [cho][nle]: black points are experimental data, red lines are theoretical functions.

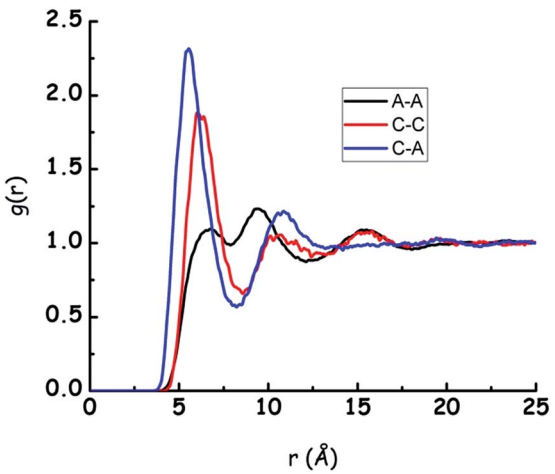

Fig. 3 Pair correlation functions between ionic species centres of masses: A–A (anion–anion), C–C (cation–cation), C–A (cation–anion).

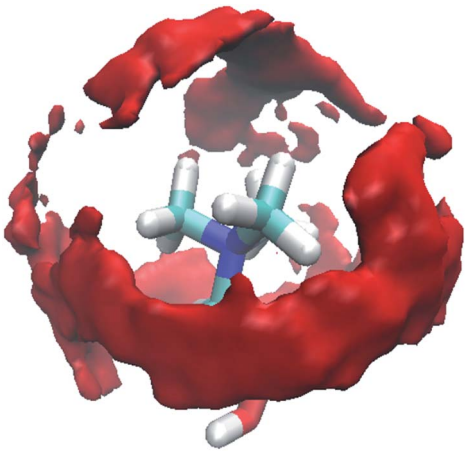

Fig. 4 Cation–Cation interactions – spatial distribution function between the ammonium head of cation (centre blue) and hydroxyl oxygen (red) of the first neighbour cation (see text).

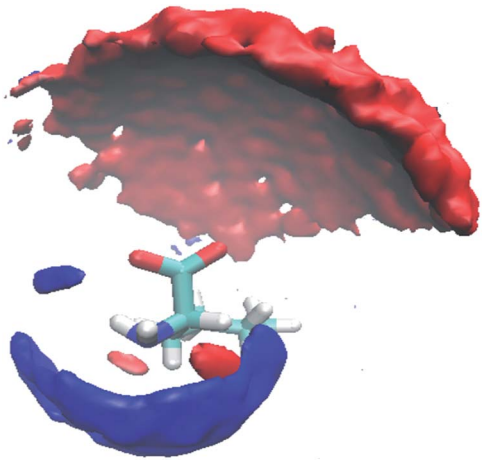

Fig. 5 Anion–Anion interactions – spatial distribution function between the anion's carboxylic unit (red) and NH_2 amine group (blue).

A) ≈ 3.9. Overall, we can anticipate that the bulk morphology of the [cho][nle] will be characterised by correlation between ionic species tending to accommodate charged moieties in a onion-like fashion; while at a larger spatial scale, the polar/apolar alternation will dominate inducing the characteristic segregation that is commonly found in ILs.

Cation–cation correlations

As shown in Fig. 3, cation–cation (C–C) correlations are quite remarkable in the present system. In particular the NC–OC $g(r)$ (see Fig. 1) is characterised by a distinct, intense (amplitude ∼ 2) peak centred at *ca.* 4.45 Å (data not shown).

In order to rationalise the potential anisotropy of the coordination highlighted in Fig. 3, we evaluated the intermolecular spatial distribution function (sdf) of OC around a reference choline moiety. This is depicted in Fig. 4. It can be appreciated that the first coordination shell corresponds to a non-negligible intermolecular correlation between the two extremes of the cation, namely the ammonium head is surrounded by the hydroxyl group. Such coordination will eventually compete with the cation–anion correlation, as we will show later.

Anion–anion correlations

As can be appreciated from the inspection of Fig. 3, anion–anion correlations are the weakest among the ones between the ionic moieties. Apart from two weak peaks centred at *ca.* 6.7 and 9.0 Å, there is no evidence of strong coordination between anions. The sdf provides indication on which correlation might be of relevance between the negatively charged ions. In Fig. 5 we report the sdf plots where the amino nitrogen (blue) and the carboxyl oxygen (red) localization volumes around a reference anion are shown. One can appreciate that enhanced distribution probabilities are detected for the species close to the amino and carboxyl groups, respectively. These are expected to be the strongest interactions between anions. Here we also note the existence of intramolecular correlations between the amino group (NL) and the carboxyl (OL) one.

We determined the rdf corresponding to this intramolecular interaction that turns out to make the anion's head pretty rigid, being characterised by a NL–OL $g(r)$ peak at a distance of 2.95 Å and a most probable angle OL···H–NL of *ca.* 91°.

Finally we mention that among anion–anion correlations, the dispersive interactions mediated correlation between alkyl tails is noteworthy and will be discussed in a separate section dealing with mesoscopic organization.

Cation–anion correlations

Being composed of ionic species, it can be easily envisaged that the main structural correlations in the [cho][nle]-IL sample are the ones between oppositely charged ions. Choline-based AA-ILs have been found to be characterised by a strong correlation between the anion carboxyl group and the cation's hydroxyl group.[22,58] Data reported in Fig. 3 for the ions' centre of mass confirm such a picture, but the structural complexity of the ions involved in the present AA-IL requires a more thorough investigation of the nature of cation–anion interactions. In Fig. 6, we show the combined distribution function (cdf) obtained considering the joint rdf and adf (pair and angular distribution functions, respectively) for OL–OC and OL···HC–OC. This cdf depicts the features of the hydrogen bonding between the two ions that is found to be very short and linear thus satisfying the conditions for a strong HB. On average 1.3 OLs are found in the first shell around the cation's hydroxyl group. An additional site exists on the anion that could interact with the cation's hydroxyl group, namely the amino group, identified with the nitrogen atom NL. In Fig. 7, we show the cdf (rdf (NL–OC) *vs.* adf (NL···HC–OC)) related to the HB between these sites. It can be appreciated that a distinct degree of HB exists between these sites as well, thus further enhancing the structural complexity of this system; we stress however that only <0.1 Hs can be detected in the first solvation shell around the amino group NL.

We also explored the correlation between the cation's ammonium and the anion's carboxyl group. There are two

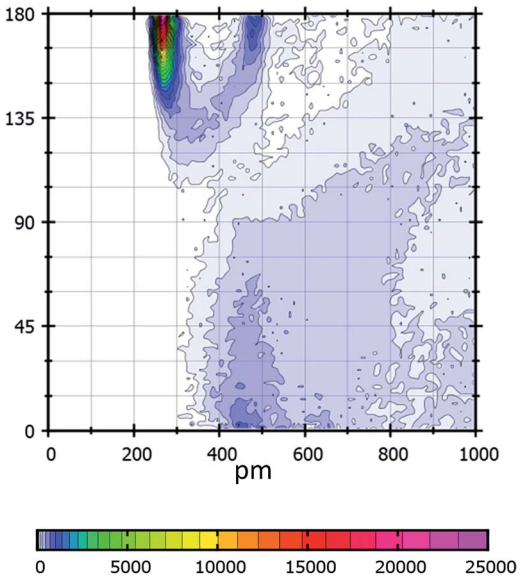

Fig. 6 Anion–cation interaction between carboxyl oxygens and hydroxyl group: combined radial/angular distribution function (cdf) of the OL–OC and OL···HC–OC correlation (x – rdf(r) in pm, y – adf).

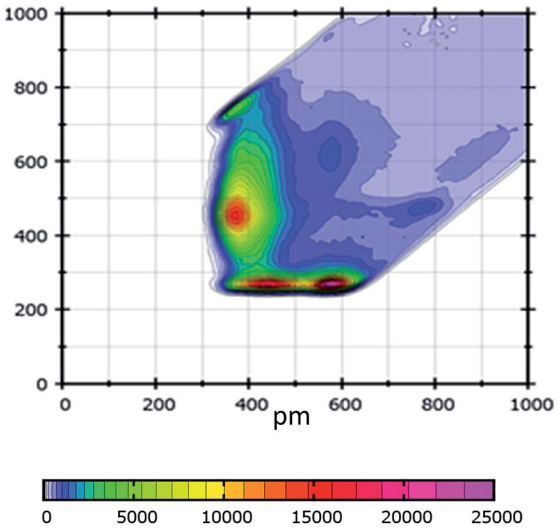

Fig. 8 Combined radial distribution functions rdf(r) for OL–OC (y-axis) and OL–NC (x-axis). Simultaneous correlations indicates the bidentate nature of anion's coordination of cation. While the first of carboxylic oxygen (OL) builds HB with the choline hydroxyl unit (OC), the second (OL) simultaneously interacts with the cation's ammonium head (NC).

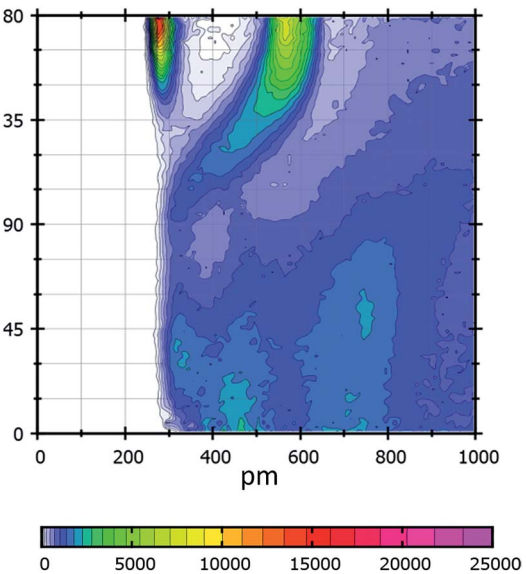

Fig. 7 Anion–cation interaction between amine group NH_2 of anion and cation's hydroxyl group: combined radial/angular distribution function (cdf) of rdf (NL–OC) *vs.* adf (NL···HC–OC) (x – rdf(r) in pm, y – adf).

different correlation peaks in the corresponding rdf, namely at *ca.* 4 and 6 Å, respectively. By evaluating the cdf for the OL–NC and OL–OC rdf's, we obtain the results of Fig. 8, where it emerges that the carboxyl unit can interact in a bidentate way with a choline cation, namely one of the carboxyl oxygen atoms will be hydrogen bonded with the hydroxyl group (r [OL–OC] ~2.5 Å) and the other will be interacting with the ammonium nitrogen (r [OL–NC] ~4.5 Å). Similar coordination was proposed for other [cho]-based AA-ILs on the basis of *ab initio* calculations.[58]

We also observed a relatively high probability for the existence of complex clusters where one bidentate anion simultaneously coordinates two different cations at the hydroxyl group, with the two OL units. In particular considering that the hydrogen bonded cation–anion pair is characterised by a distance r [CO–OC] = 3.5 Å with the first shell of solvation ending at *ca.* 4.3 Å, we detected 28%, 45%, 22% and 4.5% probability of getting 0, 1, 2, 3 OC neighbours by a distance shorter than 4.3 Å from a reference CO in the anion. This indicates the existence of a numerous population of those clusters with two cations simultaneously coordinated by one anion through HB.

Mesoscopic organization

Driven by the experimental finding of the low Q diffraction peak centred at *ca.* 0.35 $Å^{-1}$ (Fig. 2) we can safely consider that the morphology of [cho][nle] is characterised by a high degree of polar/apolar alternation, similarly to other related cases. This important finding is the consequence of the existence of a long enough alkyl tail in the [nle] moiety that leads to the chain segregation from the charged matrix leading to the formation of oily drops.[30] Considering the bio-compatible nature of the [cho]-based AA-ILs, the existence of such a thermodynamically stable nano-segregation can turn out to be very important in the development of biologically related processes in this medium. Together with the low Q diffraction feature in X-ray/neutron diffraction patterns that fingerprints the existence of such a kind segregation, one of the most commonly used indicator of this phenomenology is the pair distribution function of the terminal methyl group in the anion (CT, see Fig. 1) that shows the existence of a strong correlation peak at short distances when the alkyl tails segregation occurs. In Fig. 9, we show this $g(r)$ and one can notice the existence of a peak centred at *ca.* 4.3 Å with a large amplitude (>2.0). This correlation corresponds to

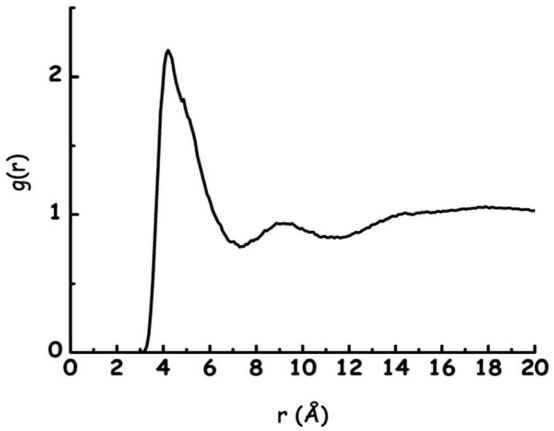

Fig. 9 Partial distribution function for terminal methyl groups of the anions alkyl chain (CT–CT). The presence of the sharp peak at around 4.5 Å reflects the strong correlations between anion's alkyl tails (see text).

an average number of five methyl groups building up the first coordination shell (up to 7.5 Å) around a reference terminal methyl group. This feature is comparable to similar ones observed in the case of various alkyl tail bearing ILs that are characterised by the polar–apolar structural dualism.[28,35,37,59] One can then assess that the nature of the low *Q* peak in this AA-IL is the same as found in more traditional ILs, where the segregation of the apolar side alkyl chains leads to the formation of domains that structurally differentiate from the 3-dimensional matrix built up by the charged moieties. We stress that apart from a study in [cho][pro][23] (where [pro] corresponds to the proline AA and does not bear an alkyl tail, but rather a cyclic moiety), previously no other AA-ILs were individuated where the alkyl tail succeeded in delivering the formation of structural heterogeneities. The previous studies on [cho][ala][22] and on other AAs[24] highlighted the featureless nature of the low *Q* portion of the diffraction patterns for these AA-based ILs.

Conclusions

We have elucidated the structure of [cho][nle] bio-degradable ionic liquid rationalizing X-ray diffraction data by means of atomistic molecular dynamics simulation and obtaining detailed information about the morphology of this system. While the strong HB formation between the AA carboxyl unit and choline hydroxyl group determines the anion–cation interaction, many other peculiar interactions have been observed. The bidentate nature of the carboxyl unit is involved in two kind of interactions: (1) one anion coordinates one cation interacting simultaneously with hydroxyl and ammonium group of cation (leading to the formation of 1 : 1 complex); (2) one anion coordinates two different cations by mean of OL$\cdots$HC interactions (leading to the formation of 1 : 2 complex). Furthermore we have shown the rather strong cation–cation correlation *via* the interaction between the ammonium and the hydroxyl groups.

The medium length alkyl tail of the n-leucine leads to the development of a characteristic polar *vs.* apolar alternation, as a consequence of the alkyl tails segregation into domains, thus delivering to the formation of an enhanced level of mesoscopic organization in this system, similarly to the structure of more conventional ILs. This is the first study, where such a mesoscopic scale structural complexity has been shown for choline–amino acids ILs. The structural dependence from the choice of AA and the length of the site alkyl chain, as well as its implication on the physicochemical properties and on solvation performance of these ILs are the subjects of our further studies.

Acknowledgements

The authors acknowledge Prof. Ruggero Caminiti (Chemistry Dept., Sapienza Univ. of Rome) for providing free computing time on NARTEN Cluster HPC Facility.

References

1 R. D. Rogers and K. R. Seddon, *Science*, 2003, **302**, 792–793.
2 M. Deetlefs, K. R. Seddon and M. Shara, *Phys. Chem. Chem. Phys.*, 2006, **8**, 642–649.
3 K. R. Seddon, *J. Chem. Technol. Biotechnol.*, 1997, **50**, 351–356.
4 M. J. Earle and K. R. Seddon, *Pure Appl. Chem.*, 2000, **72**, 1391–1398.
5 S. G. Cull, J. D. Holbrey, V. Vargas-Mora, K. R. Seddon and G. J. Lye, *Biotechnol. Bioeng.*, 2000, **69**, 227–233.
6 N. V. Plechkova and K. R. Seddon, *Chem. Soc. Rev.*, 2008, **37**, 123–150.
7 M. Petkovic, K. R. Seddon, L. P. N. Rebelo and C. Silva Pereira, *Chem. Soc. Rev.*, 2011, **40**, 1383–1403.
8 T. P. T. Pham, C.-W. W. Cho, Y.-S. S. Yun, T. P. Thuy Pham, C.-W. W. Cho and Y.-S. S. Yun, *Water Res.*, 2010, **44**, 352–372.
9 J. Arning, S. Stolte, A. Böschen, F. Stock, W.-R. Pitner, U. Welz-Biermann, B. Jastorff and J. Ranke, *Green Chem.*, 2008, **10**, 47–58.
10 M. Alvarez-Guerra and A. Irabien, *Green Chem.*, 2011, **13**, 1507.
11 G. Tao, L. He, W. Liu, L. Xu, W. Xiong, T. Wang and Y. Kou, *Green Chem.*, 2006, **8**, 639–646.
12 G.-H. Tao, L. He, N. Sun and Y. Kou, *Chem. Commun.*, 2005, 3562.
13 K. Fukumoto, M. Yoshizawa and H. Ohno, *J. Am. Chem. Soc.*, 2005, **127**, 2398–2399.
14 H. Ohno and K. Fukumoto, *Acc. Chem. Res.*, 2007, **40**, 1122–1129.
15 P. Moriel, E. J. García-Suárez, M. Martínez, a. B. García, M. a. Montes-Morán, V. Calvino-Casilda and M. a. Bañares, *Tetrahedron Lett.*, 2010, **51**, 4877–4881.
16 C. Ruß and B. König, *Green Chem.*, 2012, **14**, 2969.
17 N. Muhammad, Z. B. Man, M. A. Bustam, M. I. A. Mutalib, C. D. Wilfred and S. Rafiq, *J. Chem. Eng. Data*, 2011, **56**, 3157–3162.
18 S. De Santis, G. Masci, F. Casciotta, R. Caminiti, E. Scarpellini, M. Campetella and L. Gontrani, *Phys. Chem. Chem. Phys.*, 2015, **17**, 20687–20698.

19 X.-D. Hou, T. J. Smith, N. Li and M.-H. Zong, *Biotechnol. Bioeng.*, 2012, **109**, 2484–2493.
20 Q.-P. Liu, X.-D. Hou, N. Li and M.-H. Zong, *Green Chem.*, 2012, **14**, 304–307.
21 X.-D. Hou, Q.-P. Liu, T. J. Smith, N. Li and M.-H. Zong, *PLoS One*, 2013, **8**, e59145.
22 M. Campetella, E. Bodo, R. Caminiti, a. Martino, F. D'Apuzzo, S. Lupi and L. Gontrani, *J. Chem. Phys.*, 2015, **142**, 234502.
23 M. Campetella, S. De Santis, R. Caminiti, P. Ballirano, C. Sadun, L. Tanzi and L. Gontrani, *RSC Adv.*, 2015, **5**, 50938–50941.
24 S. E. Norman, a. H. Turner and T. G. a. Youngs, *RSC Adv.*, 2015, **5**, 67220–67226.
25 C. Herrera, G. Garcia, M. Atilhan and S. Aparicio, *J. Mol. Liq.*, 2016, **213**, 201–212.
26 A. Triolo, O. Russina, H.-J. Bleif and E. Di Cola, *J. Phys. Chem. B*, 2007, **111**, 4641–4644.
27 A. Triolo, O. Russina, B. Fazio, G. B. Appetecchi, M. Carewska and S. Passerini, *J. Chem. Phys.*, 2009, **130**, 1645211–1645216.
28 O. Russina and A. Triolo, *Faraday Discuss.*, 2012, **154**, 97–109.
29 O. Russina, F. Lo Celso, M. Di Michiel, S. Passerini, G. B. Appetecchi, F. Castiglione, A. Mele, R. Caminiti and A. Triolo, *Faraday Discuss.*, 2013, **167**, 499.
30 O. Russina, A. Triolo, L. Gontrani and R. Caminiti, *J. Phys. Chem. Lett.*, 2012, **3**, 27–33.
31 O. Russina, R. Caminiti, A. Triolo, S. Rajamani, B. Melai, A. Bertoli and C. Chiappe, *J. Mol. Liq.*, 2013, **187**, 252–259.
32 C. S. Santos, N. S. Murthy, G. a. Baker and E. W. Castner, *J. Chem. Phys.*, 2011, **134**, 1211011–1211014.
33 S. Li, J. L. Bañuelos, J. Guo, L. M. Anovitz, G. Rother, R. W. Shaw, P. C. Hillesheim, S. Dai, G. A. Baker and P. T. Cummings, *J. Phys. Chem. Lett.*, 2012, **3**, 125.
34 K. Fujii, R. Kanzaki, T. Takamuku, Y. Kameda, S. Kohara, M. Kanakubo, M. Shibayama, S. Ishiguro and Y. Umebayashi, *J. Chem. Phys.*, 2011, **135**, 244502.
35 R. Hayes, S. Imberti, G. G. Warr and R. Atkin, *Phys. Chem. Chem. Phys.*, 2011, **13**, 3237–3247.
36 O. Russina, A. Mariani, R. Caminiti and A. Triolo, *J. Solution Chem.*, 2015, **44**, 669–685.
37 H. K. Kashyap, J. J. Hettige, H. V. R. Annapureddy and C. J. Margulis, *Chem. Commun.*, 2012, **48**, 5103–5105.
38 J. C. Araque, J. J. Hettige and C. J. Margulis, *J. Phys. Chem. B*, 2015, **119**, 12727–12740.
39 H. K. Kashyap, C. S. Santos, R. P. Daly, J. J. Hettige, N. S. Murthy, H. Shirota, E. W. Castner and C. J. Margulis, *J. Phys. Chem. B*, 2013, **117**, 1130–1135.
40 O. Russina, A. Sferrazza, R. Caminiti and A. Triolo, *J. Phys. Chem. Lett.*, 2014, **5**, 1738–1742.
41 O. Russina, R. Caminiti, T. Méndez-Morales, J. Carrete, O. Cabeza, L. J. Gallego, L. M. Varela and A. Triolo, *J. Mol. Liq.*, 2015, **205**, 16–21.
42 O. Russina, M. Macchiagodena, B. Kirchner, A. Mariani, B. Aoun, M. Russina, R. Caminiti and A. Triolo, *J. Non-Cryst. Solids*, 2015, **407**, 333–338.
43 L. M. Varela, T. Méndez-Morales, J. Carrete, V. Gómez-González, B. Docampo-Álvarez, L. J. Gallego, O. Cabeza and O. Russina, *J. Mol. Liq.*, 2015, **210**, 178–188.
44 D. Atzei, T. Ferri, C. Sadun, P. Sangiorgio and R. Caminiti, *J. Am. Chem. Soc.*, 2001, **123**, 2552–2558.
45 V. R. Albertini, L. Bencivenni, R. Caminiti, F. Cilloco and C. Sadun, *J. Macromol. Sci., Part B: Phys.*, 1996, **35**, 199–213.
46 L. Gontrani, O. Russina, F. C. Marincola and R. Caminiti, *J. Chem. Phys.*, 2009, **131**, 244503.
47 M. Brehm and B. Kirchner, *J. Chem. Inf. Model.*, 2011, **51**, 2007–2023.
48 M. Brehm, H. Weber, M. Thomas, O. Hollóczki and B. Kirchner, *ChemPhysChem*, 2015, **16**, 3271–3277.
49 O. Hollóczki, M. Macchiagodena, H. Weber, M. Thomas, M. Brehm, A. Stark, O. Russina, A. Triolo and B. Kirchner, *ChemPhysChem*, 2015, **16**, 3325–3333.
50 D. A. Case, T. E. Cheatham, T. Darden, H. Gohlke, R. Luo, K. M. Merz, A. Onufriev, C. Simmerling, B. Wang and R. J. Woods, *J. Comput. Chem.*, 2005, **26**, 1668–1688.
51 J. M. Wang, R. M. Wolf, J. W. Caldwell, P. a. Kollman and D. a. Case, *J. Comput. Chem.*, 2004, **25**, 1157–1174.
52 J. Wang, W. Wang, P. a. Kollman and D. a. Case, *J. Mol. Graphics Modell.*, 2006, **25**, 247–260.
53 Y. Zhang and E. J. Maginn, *J. Phys. Chem. B*, 2012, **116**, 10036–10048.
54 L. Martínez, R. Andrade, E. G. Birgin and J. M. Martínez, *J. Comput. Chem.*, 2009, **30**, 2157–2164.
55 M. Brehm, H. Weber, A. S. Pensado, A. Stark and B. Kirchner, *Zeitschrift für Phys. Chemie*, 2013, **227**, 177–204.
56 O. Russina, L. Gontrani, B. Fazio, D. Lombardo, A. Triolo and R. Caminiti, *Chem. Phys. Lett.*, 2010, **493**, 259–262.
57 M. Macchiagodena, F. Ramondo, A. Triolo, L. Gontrani and R. Caminiti, *J. Phys. Chem. B*, 2012, **116**, 13448–13458.
58 A. Benedetto, E. Bodo, L. Gontrani, P. Ballone and R. Caminiti, *J. Phys. Chem. B*, 2014, **118**, 2471–2486.
59 A. Triolo, O. Russina, R. Caminiti, H. Shirota, H. Y. Lee, C. S. Santos, N. S. Murthy and E. W. Castner, *Chem. Commun.*, 2012, **48**, 4959–4961.